ARTICLES
https://doi.org/10.1038/s41567-021-01198-z

nature physics

Measurement of the proton spin structure at long distances

X. Zheng[1], A. Deur[1,2] ✉, H. Kang[3], S. E. Kuhn[4], M. Ripani[5], J. Zhang[1], K. P. Adhikari[2,4,6,50], S. Adhikari[7], M. J. Amaryan[4], H. Atac[8], H. Avakian[2], L. Barion[9], M. Battaglieri[2,5], I. Bedlinskiy[10], F. Benmokhtar[11], A. Bianconi[12,13], A. S. Biselli[14], S. Boiarinov[2], M. Bondì[5], F. Bossù[15], P. Bosted[16], W. J. Briscoe[17], J. Brock[2], W. K. Brooks[2,18], D. Bulumulla[4], V. D. Burkert[2], C. Carlin[2], D. S. Carman[2], J. C. Carvajal[7], A. Celentano[5], P. Chatagnon[19], T. Chetry[6], J.-P. Chen[2], S. Choi[3], G. Ciullo[9,20], L. Clark[21], P. L. Cole[22,23], M. Contalbrigo[9], V. Crede[24], A. D'Angelo[25,26], N. Dashyan[27], R. De Vita[5], M. Defurne[15], S. Diehl[28,29], C. Djalali[30,31], V. A. Drozdov[32], R. Dupre[19], M. Ehrhart[33], A. El Alaoui[18], L. El Fassi[6], L. Elouadrhiri[2], P. Eugenio[24], G. Fedotov[32], S. Fegan[34], R. Fersch[16,35], A. Filippi[36], T. A. Forest[23], Y. Ghandilyan[27], G. P. Gilfoyle[37], K. L. Giovanetti[38], F.-X. Girod[2,29], D. I. Glazier[21], R. W. Gothe[31], K. A. Griffioen[16], M. Guidal[19], N. Guler[4], L. Guo[2,7], K. Hafidi[33], H. Hakobyan[18,27], M. Hattawy[33], T. B. Hayward[16], D. Heddle[2,35], K. Hicks[30], A. Hobart[19], T. Holmstrom[16], M. Holtrop[39], Y. Ilieva[17,31], D. G. Ireland[21], E. L. Isupov[32], H. S. Jo[19,40], K. Joo[29], S. Joosten[33], C. D. Keith[2], D. Keller[1], A. Khanal[7], M. Khandaker[41,51], C. W. Kim[17], W. Kim[40], F. J. Klein[42], A. Kripko[28], V. Kubarovsky[2,43], L. Lanza[25], M. Leali[12,13], P. Lenisa[9,20], K. livingston[21], E. Long[39], I. J. D. MacGregor[21], N. Markov[29], L. Marsicano[5], V. Mascagna[13,44], B. McKinnon[21], D. G. Meekins[2], T. Mineeva[18], M. Mirazita[45], V. Mokeev[2,32], C. Mullen[5], P. Nadel-Turonski[2,17], K. Neupane[31], S. Niccolai[19], M. Osipenko[5], A. I. Ostrovidov[24], M. Paolone[8], L. Pappalardo[9,20], K. Park[2,40], E. Pasyuk[2], W. Phelps[7], S. K. Phillips[39], O. Pogorelko[10], J. Poudel[4], Y. Prok[1,4], B. A. Raue[2,7], J. Ritman[46], A. Rizzo[25,26], G. Rosner[21], P. Rossi[2,45], J. Rowley[30], F. Sabatié[15], C. Salgado[41], A. Schmidt[17], R. A. Schumacher[47], M. L. Seely[2], Y. G. Sharabian[2], U. Shrestha[30], S. Širca[48], K. Slifer[1,39], N. Sparveris[8], S. Stepanyan[2], I. I. Strakovsky[17], S. Strauch[31], V. Sulkosky[16], N. Tyler[31], M. Ungaro[2,43], L. Venturelli[12,13], H. Voskanyan[27], E. Voutier[19], D. P. Watts[34], X. Wei[2], L. B. Weinstein[4], M. H. Wood[31,49], B. Yale[16], N. Zachariou[34] and Z. W. Zhao[4,31]

Measuring the spin structure of protons and neutrons tests our understanding of how they arise from quarks and gluons, the fundamental building blocks of nuclear matter. At long distances, the coupling constant of the strong interaction becomes large, requiring non-perturbative methods to calculate quantum chromodynamics processes, such as lattice gauge theory or effective field theories. Here we report proton spin structure measurements from scattering a polarized electron beam off polarized protons. The spin-dependent cross-sections were measured at large distances, corresponding to the region of low momentum transfer squared between 0.012 and 1.0 GeV². This kinematic range provides unique tests of chiral effective field theory predictions. Our results show that a complete description of the nucleon spin remains elusive, and call for further theoretical works, for example, in lattice quantum chromodynamics. Finally, our data extrapolated to the photon point agree with the Gerasimov–Drell–Hearn sum rule, a fundamental prediction of quantum field theory that relates the anomalous magnetic moment of the proton to its integrated spin-dependent cross-sections.

Understanding how hadronic matter arises from its fundamental constituents—quarks and gluons—is central to the study of nuclear and particle physics. Although the strong interaction is described by quantum chromodynamics (QCD), it remains the least understood force in the 'Standard Model'. The difficulty arises because the QCD coupling constant α_s becomes large at long distances[1], making traditional perturbative expansions in powers of α_s infeasible. Consequently, complex phenomena like quark confinement are hard to understand quantitatively. The most fundamental approach to calculate QCD non-perturbatively

A full list of affiliations appears at the end of the paper.

is through lattice gauge theory[2]. A second approach is provided by effective field theories (EFTs), which maintain rigorous, traceable connections to the underlying fundamental theory. A popular approach is chiral effective field theory (χEFT)[3,4], which is constructed from hadronic degrees of freedom and incorporates the symmetries of QCD, including its approximate chiral symmetry. By making use of a perturbative expansion in small parameters, χEFT predicts experimental observables from a limited set of phenomenological inputs. Although generally successful, χEFT has been challenged by experimental data that depend explicitly on spin degrees of freedom[5,6]. This is not unprecedented; other theoretical predictions had been thought to be robust until confronted with spin observables, including parity symmetry[7], the Ellis–Jaffe spin sum rule[8], the nucleon spin asymmetry A_1 (ref. [9]) and lattice QCD calculations of the nucleon axial charge[10]. Therefore, fully understanding QCD and nuclear matter requires an extensive set of spin observables.

We report on the measurements performed using a polarized electron beam to probe polarized protons at the Thomas Jefferson National Accelerator Facility (Jefferson Lab), in Virginia, USA. We measured spin-dependent cross-sections in the nucleon resonance region at very low Q^2, that is, at long distances. Here, Q^2 is the square of the 4-momentum transferred from the electron to the proton and Q represents the inverse of the distance scale probed by the scattering. Polarized electrons with energies of 3.0, 2.3, 2.0, 1.3 and 1.1 GeV, produced by Jefferson Lab's Continuous Electron Beam Accelerator Facility (CEBAF), were scattered from a polarized proton target[11,12]. The beam polarization (P_b) was measured to be 85%, with a total uncertainty of 2%, using a Møller polarimeter[13]. The target contained granules of NH_3 that were dynamically polarized[11] at 1 K in a magnetic field of 5 T. The target polarization (P_t) varied from 75% to 90%, as monitored by NMR polarimetry. As described in the following and in the Methods, the product P_bP_t was measured to a relative precision of 2–5%. The scattered electrons were identified using the CEBAF Large Acceptance Spectrometer (CLAS)[13], which was equipped with a multi-layer drift chamber detector for charged particle tracking, a scintillator hodoscope for particle time-of-flight measurement, an electromagnetic calorimeter and a Cherenkov counter for discriminating scattered electrons from other background particles. The Cherenkov counter in one of the six sectors of CLAS was modified specifically for this experiment to detect electron scattering at angles as low as 6°. Only this sector was used to collect the inclusive electron scattering data reported here.

The dominant scattering process is one-photon exchange, in which the incident electron exchanges a single virtual photon with the nucleon of mass M (Fig. 1). The 4-momentum transferred from the electron to the nucleon is $q^\mu = k^\mu - k'^\mu = (\nu, \mathbf{q})$, in which k^μ and k'^μ are the 4-momenta of the incident and scattered electrons, respectively, and ν is the energy transfer. In the following, we describe this process using the Lorentz-invariant variables $Q^2 = -q^2$, and the Bjorken scaling variable $x \equiv -q^2/(2P\cdot q)$ or the invariant mass of the photon–nucleon system $W \equiv \sqrt{(P+q)^2} = \sqrt{P^2 + (1/x-1)Q^2}$. The inclusive electron scattering cross-section can be written as a linear combination of structure functions, among which $F_1(x,Q^2)$ and $F_2(x,Q^2)$ represent the spin-independent part of the cross-section, and the spin structure functions $g_1(x, Q^2)$ and $g_2(x, Q^2)$ describe its dependence on the beam and target spin polarization. These structure functions encode the internal structure of the target. Alternatively, one can describe the spin-dependent part of the nucleon response in terms of virtual photo-absorption asymmetries $A_1 = (g_1 - (Q^2/\nu^2)g_2)/F_1$ and $A_2 = (\sqrt{Q^2}/\nu)(g_1 + g_2)/F_1$ (ref. [14]). The polarized cross-section difference $\Delta\sigma \equiv \sigma^{\downarrow\Uparrow} - \sigma^{\uparrow\Uparrow}$, with $\uparrow\downarrow$ representing the beam helicity state and $\Uparrow\Downarrow$ the target spin orientation, is largely proportional to g_1 (or equivalently A_1F_1), with a small contribution from A_2F_1.

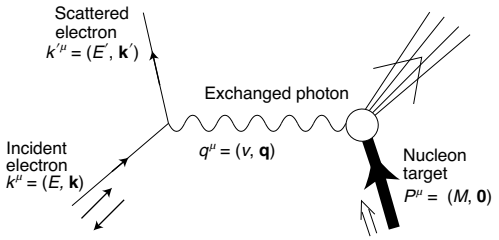

Fig. 1 | The one-photon exchange process in electron–nucleon scattering. The 4-momenta of the photon, the incident and the scattered electrons are $q^\mu = (\nu, \mathbf{q})$, $k^\mu = (E, \mathbf{k})$ and $k'^\mu = (E', \mathbf{k}')$, respectively. The spin direction of the incident electron is indicated by the arrows $\uparrow\downarrow$. The nucleon, if at rest, has $P^\mu = (M, \mathbf{0})$ and its spin is indicated by the outlined arrow $\Uparrow$.

The proton spin structure function g_1 and the product A_1F_1 were extracted from the difference in the measured yield, N, of scattered electrons from a longitudinally polarized target between opposite beam helicity states:

$$\frac{N^{\downarrow\Uparrow}}{Q_b^{\downarrow}} - \frac{N^{\uparrow\Uparrow}}{Q_b^{\uparrow}} = \Delta\sigma(W, Q^2)\mathcal{L}P_bP_t a(W, Q^2) \quad (1)$$

where Q_b is the time-integrated beam current, $\mathcal{L}$ is the areal density of polarized protons in the target, and $a(W, Q^2)$ accounts for the detector acceptance and efficiency. The product $\mathcal{L}P_bP_t$ was measured directly using elastic scattering on the proton, and $a(W, Q^2)$ was determined using a Monte Carlo simulation of the experiment (details are provided in the Methods). Examples of our g_1 results on the proton are shown in Fig. 2. The full dataset is provided in the Supplementary Information. Our results extend the measured Q^2 range down to below the pion mass squared (m_π^2), three times smaller than previous data[14–22], which makes it possible to rigorously test χEFT calculations for spin-dependent observables.

In our study, we utilize sum rules that relate integrals of structure functions to amplitudes calculable by lattice QCD[23,24] or χEFT, or to known static properties of the target. One such relation is the Gerasimov–Drell–Hearn (GDH) sum rule[25,26] for real photon absorption ($Q^2 = 0$):

$$\int_{\nu_0}^{\infty} \Delta\sigma(\nu)\frac{d\nu}{\nu} = -\frac{2\pi^2\alpha}{M^2}\kappa^2 \quad (2)$$

with κ the anomalous magnetic moment of the target particle, ν_0 the inelastic threshold and α the fine-structure constant. Theoretical arguments indicate that the divergence of the $1/\nu$ factor is compensated by the fast decrease of $\Delta\sigma$ with ν. This is supported by experiments that have verified the GDH sum rule for the proton to within ~7% accuracy[27,28]. There exist several prescriptions that generalize the GDH sum rule to electron scattering in terms of moments of spin structure functions integrated over x (which is equal to $Q^2/2M\nu$ in the laboratory frame). One often used generalization is[29]

$$\Gamma_1(Q^2) \equiv \int_0^{x_0} g_1(x, Q^2)dx = \frac{Q^2}{2M^2}I_1(Q^2) \quad (3)$$

where $x_0 = Q^2/(W_{thr}^2 - M^2 + Q^2)$ corresponds to the electroproduction threshold $W_{thr} = M + m_\pi = 1.073$ GeV. Equation (3) defines the integral I_1, which is related to the first polarized doubly-virtual Compton scattering (VVCS) amplitude that is calculable in the $\nu \to 0$ limit with lattice QCD or χEFT[3,4,30–39]. The other prevailing generalization of the GDH integral is[40]

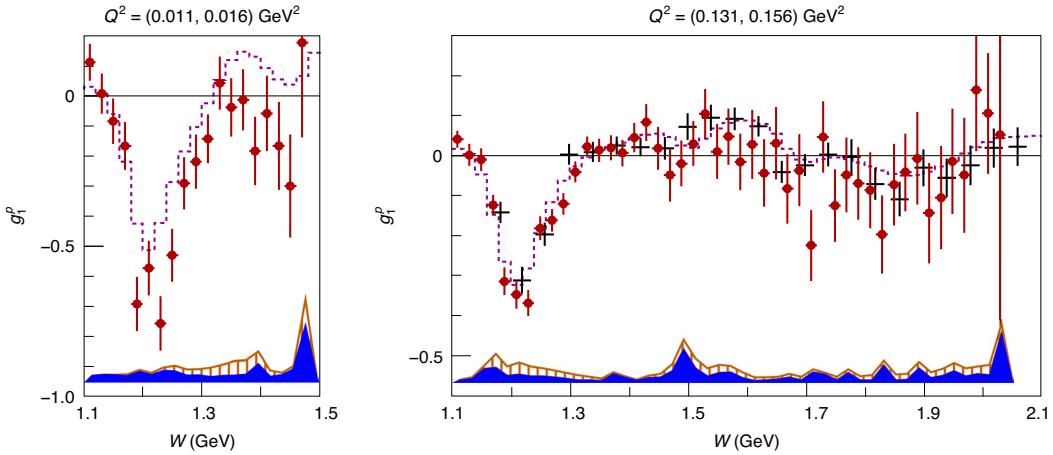

Fig. 2 | Results for $g_1(Q^2, W)$ of the proton. Data from this work (filled circles) are plotted versus invariant mass W for the lowest ($0.011 \le Q^2 \le 0.016\,\mathrm{GeV}^2$) bin and an intermediate ($0.131 \le Q^2 \le 0.156\,\mathrm{GeV}^2$) bin, compared with a parameterization of previous world data (dotted curve)[14]. The error bars are statistical. The solid and vertically hatched bands show the experimental and parameterization uncertainties, respectively. The horizontal line is the zero of the vertical axis. Results from a previous experiment carried out in Jefferson Lab's Hall B[14] are shown when available (crosses), with the error bars representing the statistical and systematic uncertainties added in quadrature.

$$I(Q^2) = \frac{2M^2}{Q^2}\int_0^{x_0}\left[A_1(x,Q^2)F_1(x,Q^2)\right]\mathrm{d}x \qquad (4)$$

which can be calculated from both the first and second spin-dependent VVCS amplitudes in the $\nu \to 0$ limit. The $I(Q^2)$ thus obtained can be extrapolated to $Q^2 = 0$ to test the original GDH prediction $I(0) = \kappa^2/4$. In this work, we present results on both generalizations.

To form the spin structure integrals in equations (3) and (4), the measured values of g_1 or A_1F_1 were used whenever available from our experiment up to a maximum x corresponding to $W = 1.15\,\mathrm{GeV}$, which was chosen to limit the background from the elastic radiative tail (Methods), and down to a minimum x determined by the beam energy and the acceptance of CLAS. Contributions from regions at low x (down to $x = 10^{-3}$) and at high x from W_{thr} to $W = 1.15\,\mathrm{GeV}$ were evaluated using a parameterization of previous data[14].

Results for $\Gamma_1(Q^2)$ and $I(Q^2)$ are shown in Figs. 3 and 4. To quantify the degree of agreement between our data and the recent χEFT predictions[36,37], we computed the χ^2 per degree of freedom between these predictions and our results. We find that the predictions in ref. [36] agree with our results only at the lowest few Q^2 points, up to $Q^2 = 0.024(0.014)\,\mathrm{GeV}^2$ for $\Gamma_1(I)$, if we require $\chi^2_{\mathrm{reduced}} < 2$. On the other hand, the predictions in ref. [37] agree with our data over their full range, with $\chi^2_{\mathrm{reduced}} < 2$ up to $Q^2 = 0.3\,\mathrm{GeV}^2$. The phenomenological models[41,42] agree well with our results for all Q^2 values. The new results on $\Gamma_1(Q^2)$ generally agree with a previous experiment[14] in the overlapping Q^2 region. However, there are visible differences between our results and the spin structure function parameterization[14], indicating that it can be improved with our data. Extrapolating our results on $I(Q^2)$ to $Q^2 = 0$ yields

$$I^{\mathrm{exp}}(0) = -0.798 \pm 0.042 \qquad (5)$$

assuming the Q^2-dependence of I predicted by Alarcón et al.[37] within their quoted theoretical uncertainty (details are provided in the Methods). This result is in good agreement with the GDH sum rule prediction $I^{\mathrm{GDH}} = -\kappa^2/4 = -0.804(0)$ for the proton and with the experimental photoproduction result $-0.832 \pm 0.023(\mathrm{stat}) \pm 0.063(\mathrm{syst})$[27,28]. Our results provide a test of the GDH sum independent of exclusive photoproduction[27,28].

Predictions from χEFT for $I(Q^2)$ and $\Gamma_1(Q^2)$ are constrained at $Q^2 = 0$ by the GDH sum rule. No such constraint is available for $\gamma_0(Q^2)$, the generalized longitudinal spin polarizability, which is related by a sum rule to the integral of A_1F_1 (refs. [40,43]):

$$\gamma_0(Q^2) = \frac{16\alpha M^2}{Q^6}\int_0^{x_0} x^2 A_1(x,Q^2)F_1(x,Q^2)\mathrm{d}x. \qquad (6)$$

This endows $\gamma_0(Q^2)$ with additional resolving power to test the several theoretical predictions available. Furthermore, the x^2 weighting in equation (6) suppresses the low-x contribution. This is beneficial, because the low-x region is inaccessible experimentally and must be estimated using models, which introduces model uncertainty. The two integrals I and γ_0 have different systematic uncertainties and therefore provide complementary tests of theoretical predictions.

Our results for $\gamma_0(Q^2)$ are shown in Fig. 5. Neither of the new χEFT calculations describes the full dataset well: the calculation from ref. [36] agrees in magnitude (but not in slope) with our lowest Q^2 results up to $Q^2 \approx 0.025\,\mathrm{GeV}^2$, while the calculation from ref. [37] describes the shape of the data only marginally below that Q^2 value. Together with the photoproduction data point[27,28,44], our data indicate a strong change in Q^2 slope towards a value consistent with that predicted in ref. [36] at very low Q^2. Classically, γ_0 represents the distortion of the proton spin structure in response to the interference between various transverse electric and magnetic field components of the virtual photon shown in Fig. 1. In a hadronic picture, γ_0 is principally due to the difference between the contribution from the pion cloud of the proton (positive) and the proton's first excited state (negative), called the Δ resonance[37]. The data thus indicate that the Δ contribution dominates at the photon point and becomes even more important for small-Q^2 virtual photons. This may be pictured intuitively from the extended size of the pion cloud, whose contribution is quickly suppressed with increasing Q^2. However, at higher Q^2, the slope turns over because the polarizability is a global feature of the proton that must vanish as $Q^2 \to \infty$, as seen from the $1/Q^6$ factor in equation (6).

Although the upper bound of the validity domain of χEFT is not known, the kinematic coverage of our data is well within its expected range between $m_\pi^2 \approx 0.02\,\mathrm{GeV}^2$ and the chiral symmetry breaking scale, $\Lambda_\chi^2 \approx 1\,\mathrm{GeV}^2$. The actual validity range depends on the order of the expansion parameter m_π/Λ_χ at which the

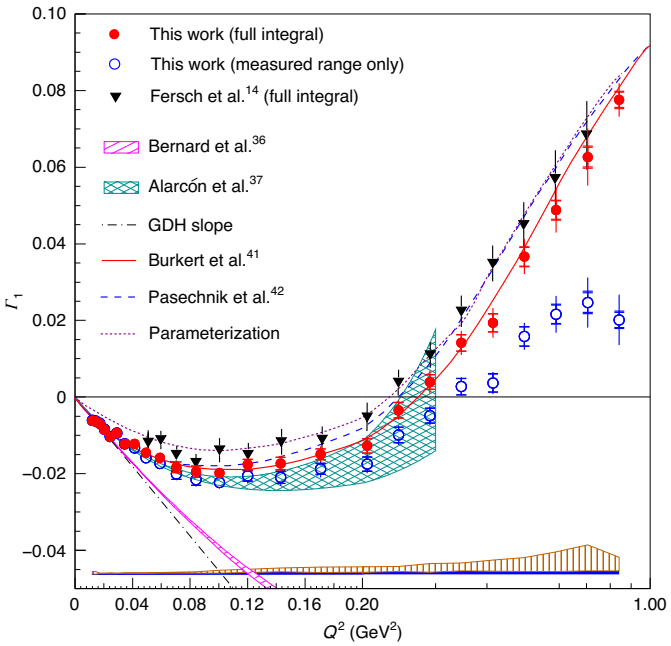

Fig. 3 | Results for $\Gamma_1(Q^2)$ for the proton. Integrals over the experimentally covered *x* range are shown as open circles. Full integrals are shown as filled circles. The inner and outer error bars (sometimes too small to be seen) are for statistical and total uncertainties, respectively. Results from a previous experiment[14] are shown as filled triangles whose error bars display the statistical and systematic uncertainties added in quadrature. The solid and vertically hatched bands show the experimental and parameterization uncertainties, respectively. Also shown are the latest χEFT predictions by Bernard et al.[36] (diagonally hatched band) and Alarcón et al.[37] (cross-hatched band), phenomenological models by Burkert et al.[41] (solid curve) and Pasechnik et al.[42] (dashed curve), as well as our spin structure function parameterization[14] (dotted curve). The dash-dotted line is the slope predicted by the GDH sum rule as $Q^2 \to 0$.

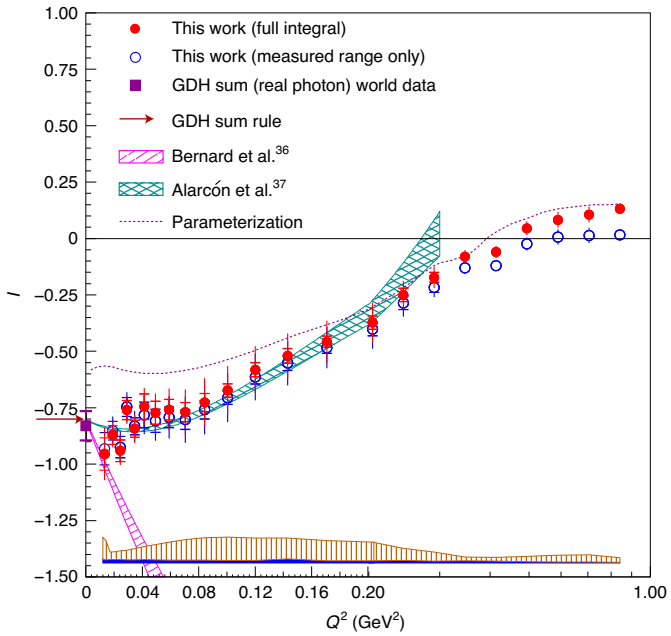

Fig. 4 | Results for $I(Q^2)$ for the proton. Integrals over the experimentally covered *x* range are shown as open circles. Full integrals are shown as filled circles. The inner and outer error bars (sometimes too small to be seen) are for statistical and total uncertainties, respectively. The solid and vertically hatched bands show the experimental and parameterization uncertainties, respectively. Also shown are the latest χEFT predictions by Bernard et al.[36] (diagonally hatched band) and Alarcón et al.[37] (cross-hatched band) and our spin structure function parameterization[14] (dotted curve). The GDH value is shown by the arrow at $I^{GDH} = -0.804$. The experimental photoproduction result[27,28] is shown by the filled square with the error bar providing the statistical and systematic uncertainties added in quadrature.

calculations are done, the expansion method and the observable. One reason for the limited success of χEFT in describing our results may be coming from the difficulty to fully account for the Δ resonance. In fact, early χEFT calculations[30–32] did not explicitly include the Δ excitation, which slows down the convergence of the χEFT perturbation series, or they included it phenomenologically[33–35]. This was thought to be the reason why many of the early nucleon spin structure function data[15–22] disagreed with calculations[30–35]. This disagreement prompted refined χEFT calculations[36–39] and an experimental programme at Jefferson Lab optimized to cover the χEFT domain[45,46], including the measurement reported here. The latest calculations[36–39] both include the Δ but differ in their expansion method to account for the π–Δ corrections. Reference [36] treats the nucleon-Δ mass difference δM as a small parameter of the same order as m_π. References [37–39] use δM as an intermediate scale such that $\delta M/\Lambda_\chi \approx m_\pi/\delta M$ is used as the expansion parameter to account for the Δ. In addition, the calculations[37–39] include empirical form factors in the relevant couplings to approximate the expected impact of high-order contributions. They make γ_0 vanish at large Q^2, as observed, in contrast to the calculation[36] that purely contains terms computed with χEFT and has no free parameter that can be adjusted. For γ_0, which arises at third order in the π–N loops, there are large cancellations between the π–N loops and the Δ contribution. Therefore, the calculations are very sensitive to the expansion and renormalization scheme, and the order of the expansion. This is why γ_0 is especially well-suited to test χEFT. Finally, the integrals Γ_1 and I contain Born terms in addition to the polarizability contributions calculated in χEFT. These terms are constrained by the GDH sum rule at $Q^2 = 0$. References [37–39] assume that their Q^2 dependence follows the corresponding proton form factors. This Q^2 dependence leads to the difference with ref. [36] and the agreement with our data. We remark that the shaded theory bands in Figs. 3–5 parameterize some of the uncertainties specific to each theoretical calculation, which are different for the two approaches. We refer the reader to the original publications[36,37] for details.

Although it is essential to understand the fundamental forces of nature from first principles, such descriptions are often impossible and one must use effective theories based on the new degrees of freedom that emerge from complexity[47]. The leading effective theory for the strong interaction, χEFT, has been precisely tested by our very low Q^2 measurement of Γ_1, I and γ_0 on the proton. The test shows that it remains difficult for χEFT to precisely describe all observables in which spin degrees of freedom are explicit. It provides strong incentive for future improvements of calculations using χEFT, the leading approach to the effective theory emerging directly from QCD, and for extending the more fundamental lattice QCD calculations to the spin-dependent structure of the nucleon.

Online content

Any methods, additional references, Nature Research reporting summaries, source data, extended data, supplementary information, acknowledgements, peer review information; details of author contributions and competing interests; and statements of data and code availability are available at https://doi.org/10.1038/s41567-021-01198-z.

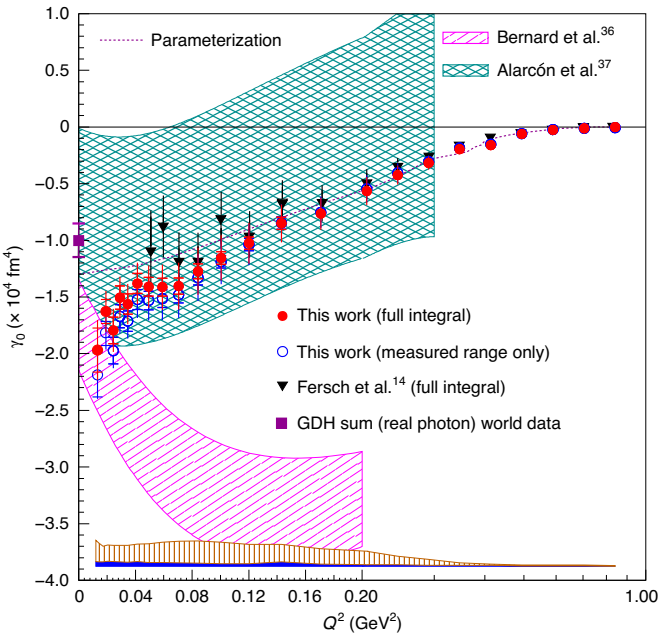

Fig. 5 | Results for $\gamma_0(Q^2)$ for the proton. Integrals over the experimentally covered x range are shown as open circles. Full integrals are shown as filled circles. The inner and outer error bars (sometimes too small to be seen) are for statistical and total uncertainties, respectively. The solid and vertically hatched bands show the experimental and parameterization uncertainties, respectively. Results from a previous experiment[14] are shown as filled triangles, whose error bars display the statistical and systematic uncertainties added in quadrature. Also shown are the latest χEFT predictions by Bernard et al.[36] (diagonally hatched band) and Alarcón et al.[37] (cross-hatched band), and our spin structure function parameterization[14] (dotted curve). The photoproduction data point[27,28,44] is shown as the filled square with the error bar providing the statistical and systematic uncertainties added in quadrature.

Received: 21 September 2020; Accepted: 4 February 2021;
Published online: 12 April 2021

References

1. Deur, A., Brodsky, S. J. & de Téramond, G. F. The QCD running coupling. *Prog. Part. Nucl. Phys.* **90**, 1–74 (2016).
2. Particle Data Group Review of particle physics. *Phys. Rev. D* **98**, 030001 (2018).
3. Bernard, V. Chiral perturbation theory and baryon properties. *Prog. Part. Nucl. Phys.* **60**, 82–160 (2008).
4. Scherer, S. Chiral perturbation theory: introduction and recent results in the one-nucleon sector. *Prog. Part. Nucl. Phys.* **64**, 1–60 (2010).
5. Kuhn, S. E., Chen, J.-P. & Leader, E. Spin structure of the nucleon—status and recent results. *Prog. Part. Nucl. Phys.* **63**, 1–50 (2009).
6. Deur, A., Brodsky, S. J. & de Téramond, G. F. The spin structure of the nucleon. *Rep. Prog. Phys.* **82**, 076201 (2019).
7. Wu, C., Ambler, E., Hayward, R., Hoppes, D. & Hudson, R. Experimental test of parity conservation in beta decay. *Phys. Rev.* **105**, 1413–1414 (1957).
8. Ellis, J. R. & Jaffe, R. L. A sum rule for deep inelastic electroproduction from polarized protons. *Phys. Rev. D* **9**, 1444–1446 (1974); erratum: **10**, 1669–1670(1974).
9. Brodsky, S. J., Burkardt, M. & Schmidt, I. QCD constraints on the shape of polarized quark and gluon distributions. *Nucl. Phys. B* **441**, 197–214 (1995).
10. Chang, C. C. et al. A percent-level determination of the nucleon axial coupling from quantum chromodynamics. *Nature* **558**, 91–94 (2018).
11. Crabb, D. G. & Day, D. B. The Virginia/Basel/SLAC polarized target: operation and performance during experiment E143 at SLAC. *Nucl. Inst. Meth. A* **356**, 9–19 (1995).
12. Keith, C. D. et al. A polarized target for the CLAS detector. *Nucl. Inst. Meth. A* **501**, 327–339 (2003).
13. Mecking, B. A. et al. The CEBAF large acceptance spectrometer (CLAS). *Nucl. Inst. Meth. A* **503**, 513–553 (2003).
14. Fersch, R. G. et al. Determination of the proton spin structure functions for $0.05 < Q^2 < 5$ GeV^2 using CLAS. *Phys. Rev. C* **96**, 065208 (2017).
15. Amarian, M. et al. The Q^2 evolution of the generalized Gerasimov–Drell–Hearn integral for the neutron using a ^{3}He target. *Phys. Rev. Lett.* **89**, 242301 (2002).
16. Amarian, M. et al. Q^2 evolution of the neutron spin structure moments using a ^{3}He target. *Phys. Rev. Lett.* **92**, 022301 (2004).
17. Amarian, M. et al. Measurement of the generalized forward spin polarizabilities of the neutron. *Phys. Rev. Lett.* **93**, 152301 (2004).
18. Deur, A. et al. Experimental determination of the evolution of the Bjorken integral at low Q^2. *Phys. Rev. Lett.* **93**, 212001 (2004).
19. Deur, A. et al. Experimental study of isovector spin sum rules. *Phys. Rev. D* **78**, 032001 (2008).
20. Dharmawardane, K. V. et al. Measurement of the x- and Q^2-dependence of the asymmetry A_1 on the nucleon. *Phys. Lett. B* **641**, 11–17 (2006).
21. Prok, Y. et al. Moments of the spin structure functions g_1^p and g_1^d for $0.05 < Q^2 < 3.0$ GeV^2. *Phys. Lett. B* **672**, 12–16 (2009).
22. Guler, N. et al. Precise determination of the deuteron spin structure at low to moderate Q^2 with CLAS and extraction of the neutron contribution. *Phys. Rev. C* **92**, 055201 (2015).
23. Chambers, A. J. et al. Nucleon structure functions from operator product expansion on the lattice. *Phys. Rev. Lett.* **118**, 242001 (2017).
24. Liang, J., Draper, T., Liu, K.-F., Rothkopf, A. & Yang, Y.-B. Towards the nucleon hadronic tensor from lattice QCD. *Phys. Rev. D* **101**, 114503 (2020).
25. Gerasimov, S. B. A sum rule for magnetic moments and the damping of the nucleon magnetic moment in nuclei. *Sov. J. Nucl. Phys.* **2**, 430–433 (1966); *Yad. Fiz.* **2**, 598–602 (1965).
26. Drell, S. D. & Hearn, A. C. Exact sum rule for nucleon magnetic moments. *Phys. Rev. Lett.* **16**, 908–911 (1966).
27. Dutz, H. et al. Experimental check of the Gerasimov–Drell–Hearn sum rule for ^{1}H. *Phys. Rev. Lett.* **93**, 032003 (2004).
28. Hoblit, S. et al. Measurements of $\vec{H}\vec{D}(\vec{\gamma},\pi)$ and implications for convergence of the Gerasimov–Drell–Hearn integral. *Phys. Rev. Lett.* **102**, 172002 (2009).
29. Ji, X.-D. & Osborne, J. Generalized sum rules for spin-dependent structure functions of the nucleon. *J. Phys. G* **27**, 127–146 (2001).
30. Bernard, V., Kaiser, N. & Meissner, U. G. Small momentum evolution of the extended Drell–Hearn–Gerasimov sum rule. *Phys. Rev. D* **48**, 3062–3069 (1993).
31. Ji, X. D., Kao, C.-W. & Osborne, J. Generalized Drell–Hearn–Gerasimov sum rule at order $O(p^4)$ in chiral perturbation theory. *Phys. Lett. B* **472**, 1–4 (2000).
32. Ji, X. D., Kao, C.-W. & Osborne, J. The nucleon spin polarizability at order $O(p^4)$ in chiral perturbation theory. *Phys. Rev. D* **61**, 074003 (2000).
33. Bernard, V., Hemmert, T. R. & Meissner, U. G. Novel analysis of chiral loop effects in the generalized Gerasimov–Drell–Hearn sum rule. *Phys. Lett. B* **545**, 105–111 (2002).
34. Bernard, V., Hemmert, T. R. & Meissner, U. G. Spin structure of the nucleon at low energies. *Phys. Rev. D* **67**, 076008 (2003).
35. Kao, C. W., Spitzenberg, T. & Vanderhaeghen, M. Burkhardt–Cottingham sum rule and forward spin polarizabilities in heavy baryon chiral perturbation theory. *Phys. Rev. D* **67**, 016001 (2003).
36. Bernard, V., Epelbaum, E., Krebs, H. & Meissner, U. G. New insights into the spin structure of the nucleon. *Phys. Rev. D* **87**, 054032 (2013).
37. Alarcón, J. M., Hagelstein, F., Lensky, V. & Pascalutsa, V. Forward doubly-virtual Compton scattering off the nucleon in chiral perturbation theory: II. Spin polarizabilities and moments of polarized structure functions. *Phys. Rev. D* **102**, 114026 (2020).
38. Lensky, V., Alarcón, J. M. & Pascalutsa, V. Moments of nucleon structure functions at next-to-leading order in baryon chiral perturbation theory. *Phys. Rev. C* **90**, 055202 (2014).
39. Lensky, V., Pascalutsa, V. & Vanderhaeghen, M. Generalized polarizabilities of the nucleon in baryon chiral perturbation theory. *Eur. Phys. J. C* **77**, 119 (2017).
40. Drechsel, D., Pasquini, B. & Vanderhaeghen, M. Dispersion relations in real, virtual Compton scattering. *Phys. Rep.* **378**, 99–205 (2003).
41. Burkert, V. D. & Ioffe, B. L. Polarized structure functions of proton and neutron and the Gerasimov–Drell–Hearn and Bjorken sum rules. *J. Exp. Theor. Phys.* **78**, 619–622 (1994).
42. Pasechnik, R. S., Soffer, J. & Teryaev, O. V. Nucleon spin structure at low momentum transfers. *Phys. Rev. D* **82**, 076007 (2010).
43. Guichon, P. A. M., Liu, G. Q. & Thomas, A. W. Virtual Compton scattering and generalized polarizabilities of the proton. *Nucl. Phys. A* **591**, 606–638 (1995).
44. Gurevich, G. M. & Lisin, V. P. Measurement of the proton spin polarizabilities at MAMI. *Phys. Part. Nucl.* **48**, 111–116 (2017).

45. Adhikari, K. P. et al. Measurement of the Q^2 dependence of the deuteron spin structure function g_1 and its moments at low Q^2 with CLAS. *Phys. Rev. Lett.* **120**, 062501 (2018).
46. Sulkosky, V. et al. Measurement of the ^{3}He spin-structure functions and of neutron (^{3}He) spin-dependent sum rules at $0.035 \leq Q^2 \leq 0.24$ GeV^2. *Phys. Lett. B* **805**, 135428 (2020).
47. Anderson, P. W. More is different. *Science* **177**, 393–396 (1972).

[1]University of Virginia, Charlottesville, VA, USA. [2]Thomas Jefferson National Accelerator Facility, Newport News, VA, USA. [3]Seoul National University, Seoul, Korea. [4]Old Dominion University, Norfolk, VA, USA. [5]INFN, Sezione di Genova, Genoa, Italy. [6]Mississippi State University, Mississippi State, MS, USA. [7]Florida International University, Miami, FL, USA. [8]Temple University, Philadelphia, PA, USA. [9]INFN, Sezione di Ferrara, Ferrara, Italy. [10]National Research Centre Kurchatov Institute – ITEP, Moscow, Russia. [11]Duquesne University, Pittsburgh, PA, USA. [12]Università degli Studi di Brescia, Brescia, Italy. [13]INFN, Sezione di Pavia, Pavia, Italy. [14]Fairfield University, Fairfield, CT, USA. [15]IRFU, CEA, Université Paris-Saclay, Gif-sur-Yvette, France. [16]College of William and Mary, Williamsburg, VA, USA. [17]The George Washington University, Washington DC, USA. [18]Universidad Técnica Federico Santa María, Valparaíso, Chile. [19]Université Paris-Saclay, CNRS/IN2P3, IJCLab, Orsay, France. [20]Università di Ferrara, Ferrara, Italy. [21]University of Glasgow, Glasgow, UK. [22]Lamar University, Beaumont, TX, USA. [23]Idaho State University, Pocatello, ID, USA. [24]Florida State University, Tallahassee, FL, USA. [25]INFN, Sezione di Roma Tor Vergata, Rome, Italy. [26]Università di Roma Tor Vergata, Rome, Italy. [27]Yerevan Physics Institute, Yerevan, Armenia. [28]II Physikalisches Institut der Universitaet Giessen, Giessen, Germany. [29]University of Connecticut, Storrs, CT, USA. [30]Ohio University, Athens, OH, USA. [31]University of South Carolina, Columbia, SC, USA. [32]Skobeltsyn Institute of Nuclear Physics, Lomonosov Moscow State University, Moscow, Russia. [33]Argonne National Laboratory, Argonne, IL, USA. [34]University of York, York, UK. [35]Christopher Newport University, Newport News, VA, USA. [36]INFN, Sezione di Torino, Turin, Italy. [37]University of Richmond, Richmond, VA, USA. [38]James Madison University, Harrisonburg, VA, USA. [39]University of New Hampshire, Durham, NH, USA. [40]Kyungpook National University, Daegu, Republic of Korea. [41]Norfolk State University, Norfolk, VA, USA. [42]Catholic University of America, Washington DC, USA. [43]Rensselaer Polytechnic Institute, Troy, NY, USA. [44]Università degli Studi dell'Insubria, Como, Italy. [45]INFN, Laboratori Nazionali di Frascati, Frascati, Italy. [46]Institute fur Kernphysik (Juelich), Juelich, Germany. [47]Carnegie Mellon University, Pittsburgh, PA, USA. [48]University of Ljubljana, Slovenia Jožef Stefan Institute, Ljubljana, Slovenia. [49]Canisius College, Buffalo, NY, USA. [50]Present address: Hampton University, Hampton, VA, USA. [51]Present address: Idaho State University, Pocatello, ID, USA. ✉e-mail: deurpam@jlab.org

Methods

We measured the spin difference yields on the left-hand side of equation (1) and solved that equation for $\Delta\sigma(W, Q^2)$, from which we extracted g_1 and A_1F_1 as functions of W and Q^2. We relied on the standard CLAS GEANT-3 Monte Carlo simulation package to fully simulate the spin-dependent yields, including all radiative effects and detector responses. The efficiency of the modified Cherenkov counter was determined by comparing data taken with only the electromagnetic calorimeter in the trigger to those taken with the standard trigger that requires a coincidence between both detectors. The ratio of the latter to the former gave the Cherenkov efficiency. We selected only detector regions of well-understood acceptance in both the data and the simulation. This process fully determined the function $a(W, Q^2)$ in equation (1). The same equation (1) was also used to extract the product $\mathcal{L}P_bP_t$ by comparing the measured yield difference (left-hand side of equation (1)), integrated over the elastic peak region $0.85\,\mathrm{GeV} < W < 1.0\,\mathrm{GeV}$, to the elastic cross-section difference $\Delta\sigma(W=M, Q^2)$, which can be calculated from the known electromagnetic form factors of the proton[48].

The polarized cross-section $\Delta\sigma(W, Q^2)$ in the simulation was calculated using an event generator for inclusive electron scattering[49] with up-to-date models of structure functions and asymmetries, including near-final data from a Jefferson Lab experiment that measured the proton structure function g_2^p. We extracted our results on g_1 and A_1F_1 by varying our input parameterization for these quantities and finding the required values to make our simulation for the polarized yield agree with data. Corrections for higher-order quantum electromagnetic effects (radiative corrections) were applied in the simulation, of which one effect is the high-energy tail from elastic scattering (elastic radiative tail).

We propagated the uncertainties on the polarized yields to the final values for g_1 and A_1F_1. Systematic uncertainties were studied by changing model parameters, or other inputs, and re-running the simulation. The overall uncertainty on the normalization factor $\mathcal{L}P_bP_t$ for each beam energy varied from 2% to 5%, dominated by the statistics of the measured elastic peak and, to a lesser extent, the accuracy of the proton elastic form factors[48] that enter into $\Delta\sigma(W=M, Q^2)$ and hence into our determination of that factor. Smaller contributions, all less than 1%, came from π^- and e^+e^- backgrounds, as well as scattering off the slightly polarized ^{15}N in the target. The reconstruction of W has an uncertainty of less than 2 MeV, which was studied by shifting the simulated W spectrum and repeating the extraction. Uncertainties due to trigger and particle reconstruction and identification inefficiencies, as well as parameterizations for the structure functions, $F_{1,2}$ and $A_{1,2}$, were studied by varying them in the simulation. Uncertainties in the radiative corrections were estimated by varying the amount of material the electron passed through in the simulation, and by adjusting the elastic radiative tail within reasonable limits. In all, the total experimental uncertainty is dominated by statistics.

To extrapolate our results on $I(Q^2)$ to $Q^2=0$, we fit our data with a form obeying the Q^2-dependence of the Alarcón et al. χEFT calculation[37]. We chose this calculation because its Q^2-dependence agrees well with our data over a wide Q^2 range. We found the intercept of our fit with the $Q^2=0$ axis to be $I^{exp}(0) = -0.798 \pm 0.013(\mathrm{uncor}) \pm 0.040(\mathrm{cor}) \pm 0.003(\mathrm{range}) \pm 0.003(\mathrm{form})$, with $\chi^2_{\mathrm{reduced}} = 2.20$ determined with the 'uncor' uncertainty. Here, 'uncor' and 'cor' refer to the experiment point-to-point uncorrelated and correlated uncertainties, respectively, and 'range' refers to the uncertainty due to the Q^2 range ($Q^2 \leq 0.1\,\mathrm{GeV}^2$) used for the fit. The last contribution, 'form', is the uncertainty on the Q^2-dependence used for the fit. It is calculated from the uncertainty band given by the χEFT calculation[37]. Because the various uncertainties are largely independent, they are added quadratically, giving a total uncertainty of ±0.042. This is about twice smaller than that from photoproduction measurements of $I(0)$ because the $Q^2 \to 0$ extrapolation uncertainty calculated using ref. [37] is negligible and because inclusive electroproduction automatically sums over all reaction channels, thereby removing uncertainties associated with the detection of final states needed in photoproduction. On the other hand, the extrapolation uncertainty is calculated from ref. [37], which disagrees with ref. [36]. This indicates that the uncertainty bands provided in the calculations may not reflect the full theoretical uncertainties. Extrapolating using the Q^2-dependence from ref. [36] yields $I^{exp}(0) = -0.625 \pm 0.022(\mathrm{uncor}) \pm 0.039(\mathrm{cor}) \pm {}^{0.069}_{0.013}(\mathrm{range}) \pm 0.056(\mathrm{form})$, with $\chi^2_{\mathrm{reduced}} = 2.23$ determined with the 'uncor' uncertainty. The 'uncor' value here is larger because the fit is limited to very few data points ($Q^2 \leq 0.024\,\mathrm{GeV}^2$). This result differs notably from our main result, as expected from the very different slope of ref. [36]. This discrepancy exemplifies the importance of testing and improving χEFT calculations, because well-controlled predictions would make electroproduction data very competitive for verifying the GDH sum rule and other real photon observables.

Data availability

Experimental data that support the findings of this study will be posted on the CLAS database (https://clasweb.jlab.org/physicsdb/) or are available from the corresponding author upon request.

Code availability

The computer codes that support the plots within this paper and the findings of this study are available from X.Z. upon request.

References

48. Arrington, J., Melnitchouk, W. & Tjon, J. A. Global analysis of proton elastic form factor data with two-photon exchange corrections. *Phys. Rev. C* **76**, 035205 (2007).
49. Abe, K. et al. Measurements of the proton and deuteron spin structure functions g_1 and g_2. *Phys. Rev. D* **58**, 112003 (1998).

Acknowledgements

All authors are members of The Jefferson Lab CLAS Collaboration. We thank the personnel of Jefferson Lab for their efforts that resulted in the successful completion of the experiment. We thank Kovacs for her contribution to the early analysis of the data. We are grateful to U.-G. Meißner and V. Pascalutsa for useful discussions on the theoretical χEFT calculations. This work was supported by the US Department of Energy (DOE), the US National Science Foundation, the US Jeffress Memorial Trust, the UK Science and Technology Facilities Council (STFC), the Italian Istituto Nazionale di Fisica Nucleare, the French Institut National de Physique Nucléaire et de Physique des Particules, the French Centre National de la Recherche Scientifique and the National Research Foundation of Korea. This material is based on work supported by the US Department of Energy, Office of Science, Office of Nuclear Physics under contract no. DE-AC05-06OR23177.

Author contributions

The members of the Jefferson Lab CLAS Collaboration constructed and operated the experimental equipment used in this experiment. A large number of collaboration members participated in the data collection. The following authors provided various contributions to the experiment design and commissioning, data processing, data analysis and Monte Carlo simulations: M. Battaglieri, R. De Vita, V. A. Drozdov, L. El Fassi, H. Kang, E. Long, M. Osipenko, S. K. Phillips and K. Slifer. The authors who performed the final data analysis and Monte Carlo simulations were A. Deur, S. E. Kuhn, M. Ripani, J. Zhang and X. Zheng. The manuscript was reviewed by the entire CLAS Collaboration before publication, and all authors approved the final version of the manuscript.

Competing interests

The authors declare no competing interests.

Additional information

Supplementary information The online version contains supplementary material available at https://doi.org/10.1038/s41567-021-01198-z.

Correspondence and requests for materials should be addressed to A.Deur.

Peer review information *Nature Physics* thanks Mohammad Ahmed and the other, anonymous, reviewer(s) for their contribution to the peer review of this work.

Reprints and permissions information is available at www.nature.com/reprints.